ACS APPLIED MATERIALS & INTERFACES

www.acsami.org

Research Article

Magnetism-Responsive Anisotropic Film with Self-Sensing and Multifunctional Shape Manipulation

Li Ding, Jingyi Zhang, Quan Shu, Siyong Liu, Shouhu Xuan, Xinglong Gong,* and Dongsheng Zhang*

Cite This: *ACS Appl. Mater. Interfaces* 2021, 13, 13724−13734

Read Online

ACCESS | Metrics & More | Article Recommendations | Supporting Information

ABSTRACT: At small scales, shape-programmable magnetic materials and self-sensing conductive materials have an enticing potential for realizing the functionalities that are unattainable by traditional machines. This work reports a facile preparation method of aself-sensing magnetism-responsive anisotropic films (SMAF) in which magnetic materials and conductive materials can be predesigned, oriented, and patterned without requiring an external magnetic field generator or other expensive devices. A variety of shaped magnetoactive films with complex chain-orientation structures that can achieve advanced actuation functions have been developed, such as magnetically driven flowers, windmills, and leaves. It is also verified that the as-prepared samples coated with the sensing layer can distinguish different actuation modes, such as inward bending, outward bending, twisting, and combined deformation, which would be conducive to further exploration and development of directionally responsive applications in the smart actuating system and soft robotics.

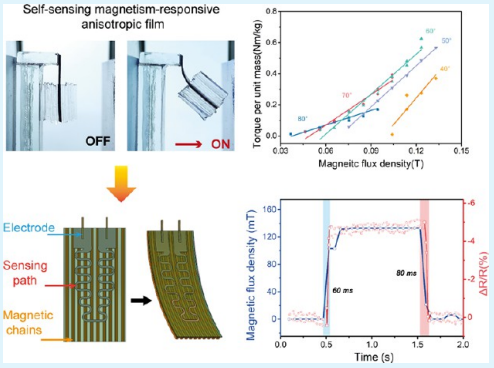

KEYWORDS: *soft robot, actuation, sensor, magnetic, smart material*

INTRODUCTION

Mollusks with unlimited degrees of freedom and continuous deformation ability can change their shape arbitrarily in a large range and are inherently highly adaptable. The bionic actuators with similar capabilities have always been the goal of researchers from all over the world.[1,2] According to the actuation mechanisms, the bionic soft actuators can be mainly divided into piezoelectric actuators,[3] electroadhesion actuators,[4] pneumatic or hydraulic actuators,[5] intelligent material-based actuators,[6,7] magnetism-responsive actuators, etc. Especially, due to the controllable mechanics, fast response, and wirelessly controlled performance in confined space, magnetorheological composite-based actuators have great development prospects in the fields of intelligent micromachinery, bionic soft robots, etc.[8−10]

The actuation behaviors of magnetorheological composites are mainly affected by the external magnetic field and the internal microstructure of the magnetic material.[11−14] It has been recognized that the orientation angles of magnetic chains can be controlled by adjusting the preloaded magnetic fields in the vulcanizing procedure.[15−17] With the use of magnetic field generators, anisotropic magnetorheological films with directional chain orientations have been developed, exhibiting diverse application potentials in soft robotics.[18−20] Most recently, two-dimensional (2D)/three-dimensional (3D) printing technology has been gradually implemented and has brought dramatic changes to the programming design of magnetic composites.[21−24] However, difficulties still exist in either incorporation of magnetic field generation equipment or facilitation of fabrication procedure for complex chain-orientation arrangements. Consequently, to date, most studies are focused on a hard magnetic actuating system or the preparation and performance characterization of soft magnetorheological composites with a simple chain orientation, while the soft magnetic composites with complex chain-orientated structures are rarely involved and using chained magnetic composites for directional and selective actuation has yet to be fully developed and optimized for soft robotic applications. Compared with hard magnetic materials, soft magnetic materials have the characteristics of low hysteresis loss, high permeability, and low coercivity. Therefore, developing an ingenious and facile manufacturing method without a magnetic field for flexible anisotropic magnetic composites and soft robots is of great significance and may provide a new solution for the next-generation magnetism-responsive actuating system.

Numerous research studies demonstrate that anisotropic magnetorheological composites have excellent contact-free magnetoinduced actuation characteristics, which has been

Received: January 26, 2021
Accepted: March 1, 2021
Published: March 10, 2021

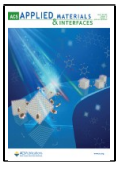

https://dx.doi.org/10.1021/acsami.1c01721
ACS Appl. Mater. Interfaces 2021, 13, 13724−13734

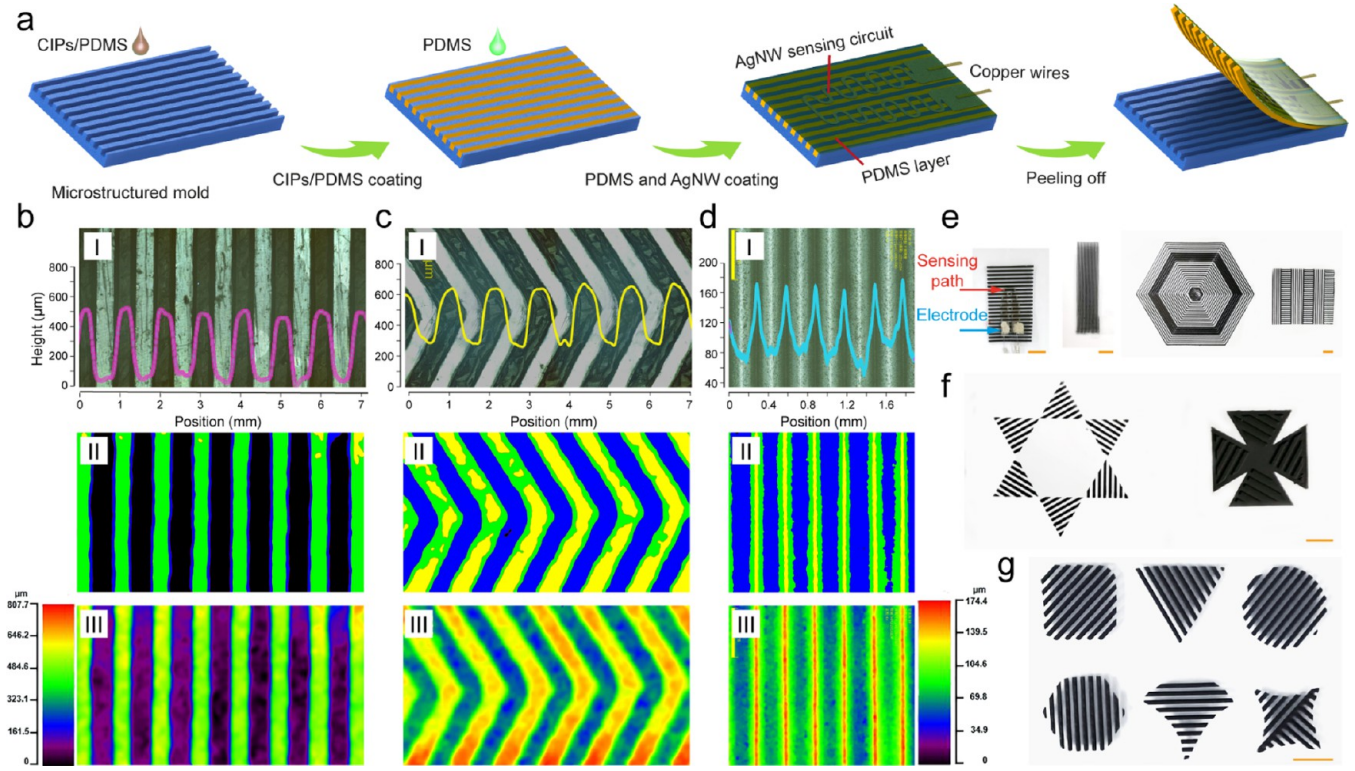

Figure 1. Fabrication process and structural characterization. (a) Schematic diagram of the fabrication steps for SMAF. (b–d) Optical microscopy images of unilaterally structured MAF with different microstructures (color map (I), profile map (II), and height map (III)). (e–g) SMAF or MAF samples of different shapes with oriented magnetic structural elements. The scale bar is 5 mm.

used to develop various functional devices, such as fertilization assistance, artificial muscles, and wireless microgrippers.[25−27] At present, the actuating systems have been undergone rapid growth;[28−30] and moreover, some of them with integrated mechanical-sensing elements can not only perform various actuating actions but also self-perceive their position, posture, and environmental change.[31−33] Particularly, as magnetism-responsive actuators have great application potentials in enclosed environments (such as blood vessels[34,35]), the magnetic actuating devices are required to monitor and feedback in real-time for operation purposes. However, most research studies on magnetism-responsive actuators are focused on the actuating performances, and only a few can feedback the execution status of the actuator.[36−40] Studies on the self-sensing and distinguishment of actuation behaviors of magnetism-responsive materials with complex chain-orientation structure are rarely reported. Therefore, how to introduce sensing units into the preparation of magnetorheological composites with complex chain-orientation structure is also worthy of exploration to understand the intrinsic relationship of the microstructure, external magnetic field, and magnetic−mechanic coupling behaviors.

In our work, a self-sensing magnetism-responsive anisotropic film (SMAF) with noncontact control and multiple driving modes has been reported through a combination of spin coating of flexible poly(dimethylsiloxane) (PDMS) matrix and soft magnetic carbonyl iron particles (CIP) with mask-patterning conductive silver nanowire (AgNW) sensing layer. The proposed fabrication method is novel, facile, nonmagnetic, cost-effective, environmental-friendly, and has structural design flexibility. Magnetoactive anisotropic composite with different chain-orientation arrangements exhibit different actuation modes, and the output electrical signals of the coated AgNW sensing layer can reflect and distinguish different actuation modes. By establishing a simple magnetic−mechanic−electric experimental platform, we investigated systematically the deformation performance and the electrical responses under tactile mechanical and contactless magnetic conditions.

RESULTS AND DISCUSSION

Fabrication and Structural Characterization. Figure 1a schematically depicts the preparation process of a self-sensing magnetism-responsive anisotropic film. The fabrication procedure is facile, freely programmable, and cost-effective and can be mass produced. It involves five main steps: (i) coating and vulcanizing of pre-CIPs/PDMS mixture on a 3D-printed microstructured mold, (ii) scraping off excess CIPs/PDMS mixture at the protrusion of master mold, (iii) spin coating and vulcanizing of the pre-PDMS mixture, (iv) coating of AgNW sensing layer using a reusable masking film, and then peeling off the masking film and the adherence of conductive electrodes, and (v) spin coating and vulcanizing of the pre-PDMS mixture. Finally, after peeling, SMAF is obtained. If the fourth operation is not performed, the final product is a magnetism-responsive anisotropic film (MAF). The preset experimental parameters, such as the microstructure of mold and mask, spinning speed, and coating times, determine the microstructure of the final product. Figure 1b–d exhibits the optical microscopy images of the MAF products with different microstructures (color map (I), profile map (II), and height map (III)). The oriented magnetic structural elements can be clearly seen. More SMAF or MAF products with different magnetic arrangement structures or different shapes are shown in Figure 1e–g.

https://dx.doi.org/10.1021/acsami.1c01721
ACS Appl. Mater. Interfaces 2021, 13, 13724−13734

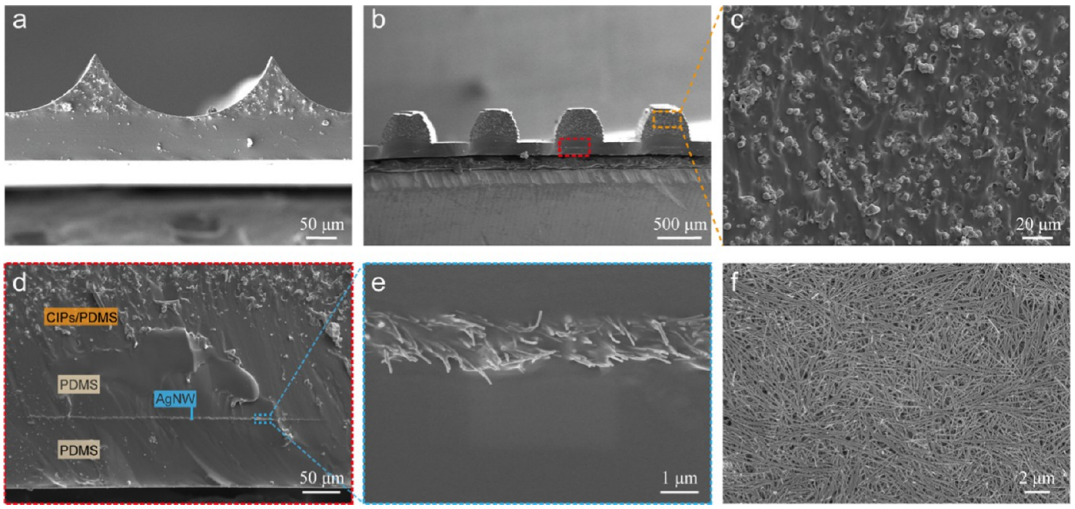

Figure 2. Material characterization of the asymmetrically structured SMAF samples. (a, b) SEM cross-sectional image of the films made with different molds. (c) SEM image of CIP embedded in the PDMS matrix. (d, e) Magnified image of the AgNW film. (f) SEM top-view image of the AgNW layer.

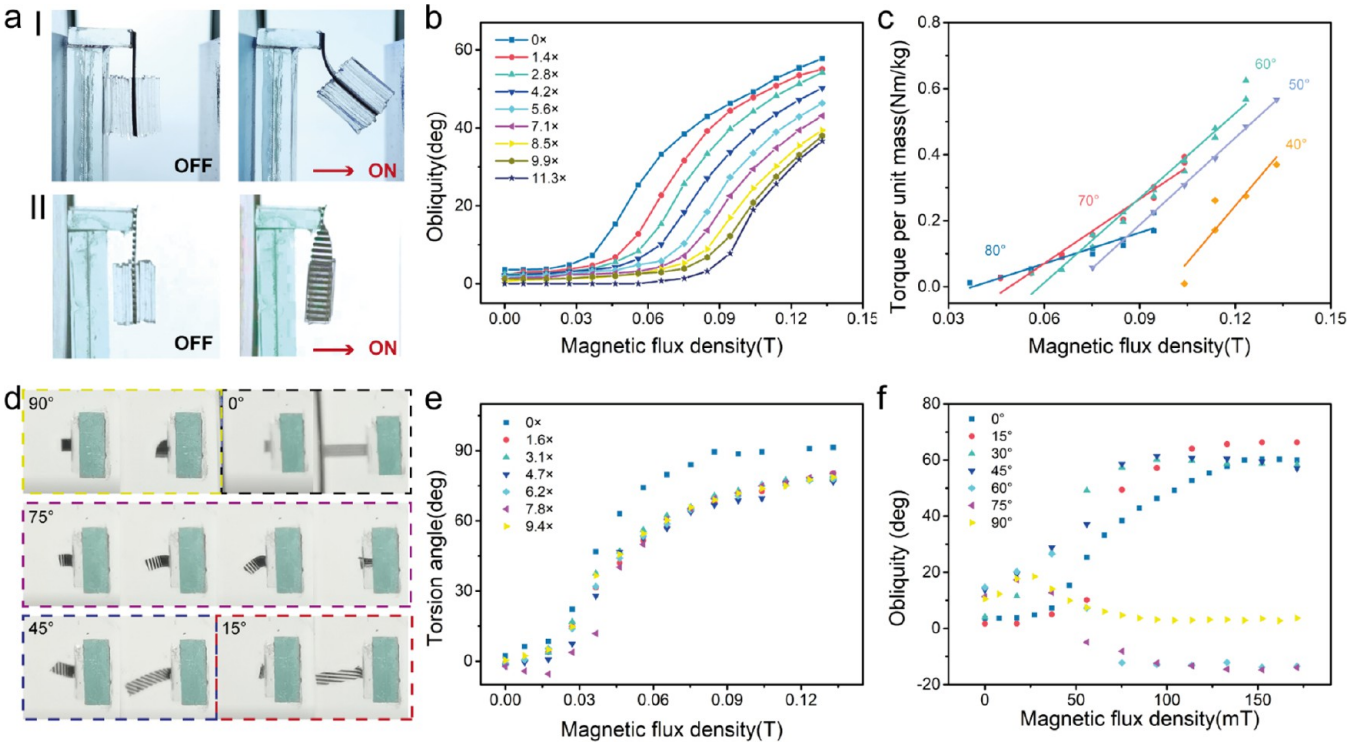

Figure 3. Magnetism-responsive actuation of MAF samples with oriented magnetic structural elements. (a) Optical images of a MAF sample with magnetic chains oriented lengthwise (I) and a MAF sample with magnetic chains oriented breadthwise (II) with one end fixed and the other end attached to pieces of PDMS plates without magnetic field (left) and under 0.13 T horizontal field (right). (b) Lifting obliquity vs applied magnetic field for MAF samples attached to the loadings. (c) Magnetic torque per unit mass of MAF vs applied magnetic field, calculated from the lifting experiments in (b). Each plot represents the magnetic torque at a different, fixed cantilever angle. (d) Optical images of MAF samples with different magnetic chain oriented angles under magnetism actuation. (e) Torsion angle vs applied magnetic field for the MAF sample with magnetic chains oriented breadthwise. (f) Dependence of lifting obliquity on the cross-angles under magnetism actuation.

Scanning electron microscopy (SEM) images (Figure 2) provide more detailed information of the micro-/nanostructure of SMAF, confirming the presence of the magnetic gratings. On the contrary, the backside of the final product is almost flat and filled with nonmagnetic particles. Figure 2a exhibits that the height of the oriented magnetic structural elements is about 100 μm and the thickness of the PDMS layer is about 60 μm. The cross-sectional image of the SMAF sample shown in Figure 2b demonstrates that the thickness of the coated PDMS film at 1250 rpm for 60 s is about 60 μm, the film thickness at 1000 rpm for 60 s is about 90 μm, and the total thickness of the SMAF sample is about 500 μm. The oriented magnetic structural elements are about 350 μm in height and about 540 μm in width. For the convenience of characterization, the MAF samples applied in other experiments were manufactured with the same height and spacing as that of oriented magnetic

https://dx.doi.org/10.1021/acsami.1c01721
ACS Appl. Mater. Interfaces 2021, 13, 13724−13734

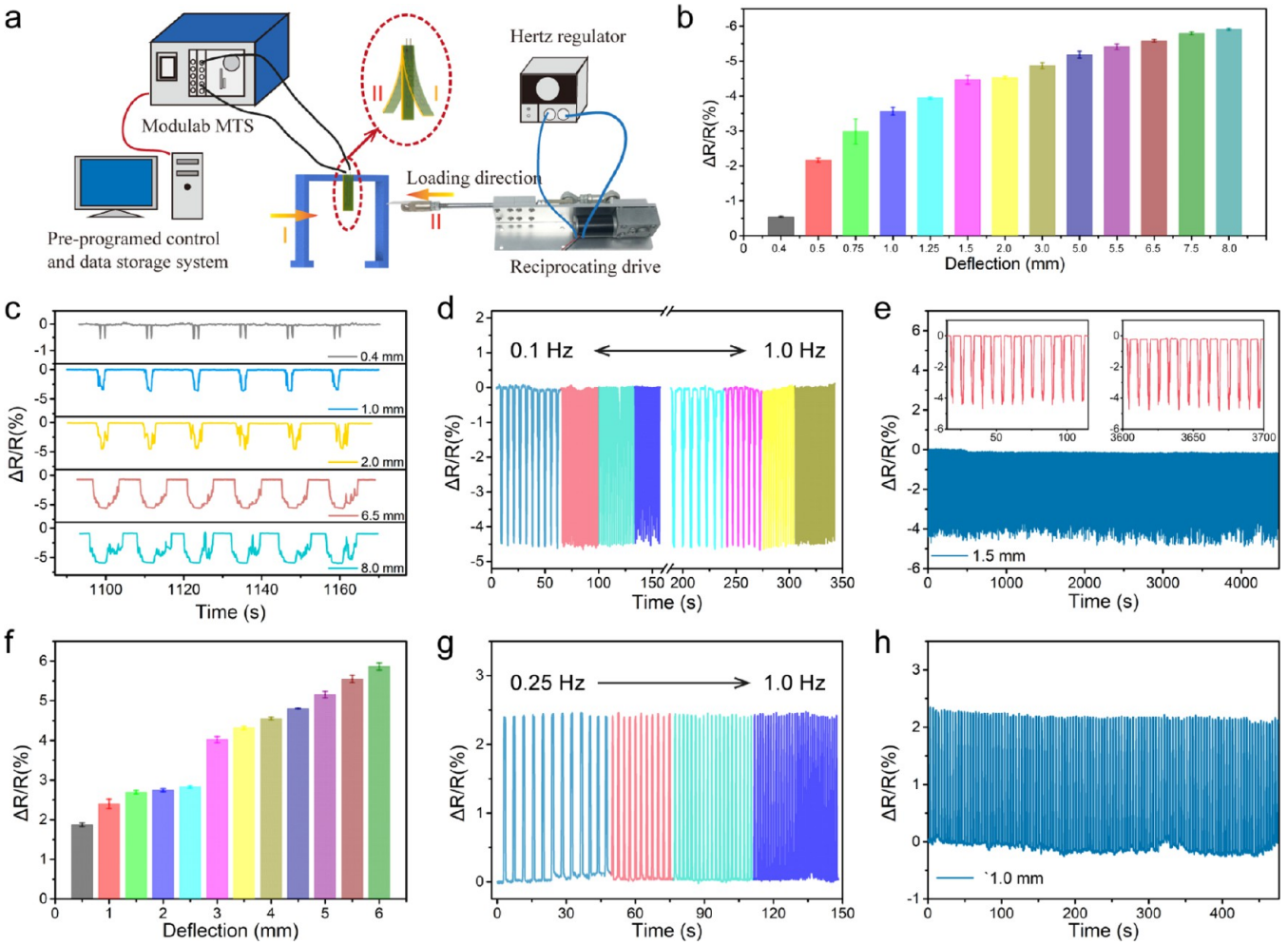

Figure 4. Mechanical−electrical responsiveness. (a) Schematic illustration of the measurement system. (b) Normalized resistance change vs the deflection at the end of SMAF sample when the drive rod was loaded from direction I. (c) Normalized resistance variation as a function of time under the deflection stimulus that incrementally increases and decreases at a frequency of 0.1 Hz. (d) $\Delta R/R$ under 1.5 mm deflection at different frequencies. (e) Real-time monitoring of normalized relative resistance in the cycled loading and unloading of drive rod from direction I. (f) $\Delta R/R$ vs the deflection when the drive rod was loaded from direction II. (g) Real-time monitoring of $\Delta R/R$ with different frequencies. (h) Cyclic test when the loading was from direction II.

structural elements and the same spin speed and coating times as shown in Figure 2b. Also, as shown in Figure 2c−e, carbonyl iron particles and AgNW sensing layer are completely embedded in the polymer matrix. It can also be clearly seen that in the width direction, the coated AgNW sensing layer is thicker in the middle than at the ends. The thickness in the middle is about 1.2 μm, and the more detailed structure is demonstrated in Figure S1. Figure 2f exhibits the top-view image of the reticulated AgNW sensing layer without polymer coverage. Figure S2 exhibits the as-prepared sample of 167 mm × 120 mm × 0.5 mm and a sample of 2.5 mm × 1.2 mm × 0.16 mm. It can be clearly seen that the magnetic particle chains along the long edge of film surface are very obvious and continuous.

Magnetism-Responsive Actuation. To characterize the magnetically dependent mechanic behavior, the hysteresis loops of the MAF samples were first measured (Figure S3). The low magnetic remanence and coercivity suggest that the MAF sample has an ideal and quick magnetic response performance. Besides, the tendency of the magnetization loops exhibits that it has high magnetic permeability and is easier to magnetize in a direction parallel to the magnetic chains. Furthermore, to analyze the responsiveness to different magnetic fields, the as-prepared magnetoactive film with oriented magnetic chains was cut into strips (length of 15 mm, width of 3.5 mm, thickness of 0.5 mm). The MAF sample was affixed to the edge of a rigid, and nonmagnetic glass holder and the weights (PDMS plate) were symmetrically attached on the underside of the strip (Figure 3a). For the MAF sample with magnetic chains oriented lengthwise, without the magnetic field, the MAF lever arm hung almost vertically, and after a horizontal magnetic field was applied, the MAF lever arm rotated upward. The experiment was repeated with different weight loads, ranging from unloaded (0×) to loading of 11.3 times the mass of the MAF sample (11.3×). By gradually increasing the magnetic flux density, the MAF sample and the attached weight can be lifted controllably. The magnetic torque was then inferred by equating it with the reverse gravity torque on the loaded lever arm. Hereby, it was considered that the system centroid was at the center of the attached weights. The lifting obliquity was defined as the angle between the vertical direction and the line of the system centroid and the hinge. Also, measurements of the position were taken under equilibrium conditions. Furthermore, by

https://dx.doi.org/10.1021/acsami.1c01721
ACS Appl. Mater. Interfaces 2021, 13, 13724−13734

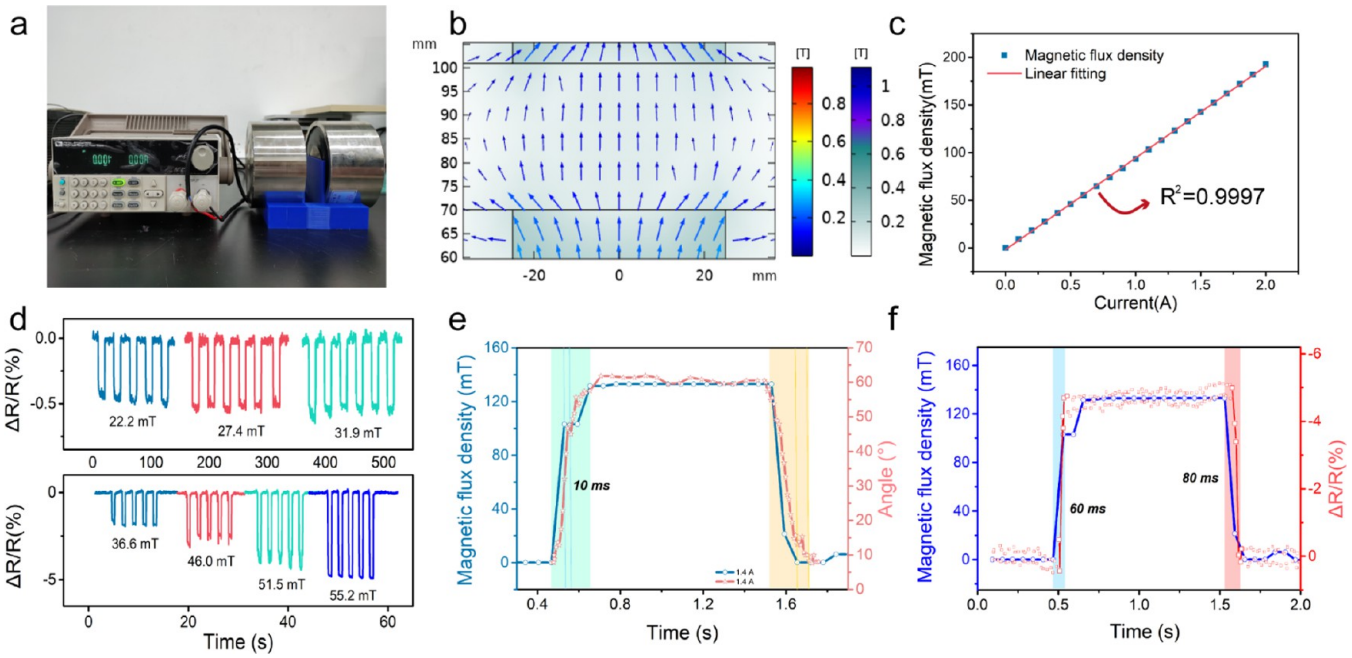

Figure 5. Magnetic−electric performance of SMAF with magnetic chains oriented lengthwise. (a, b) Electromagnetic system and the applied magnetic field which can be adjusted by the electromagnetic coil current. (c) Relationship between coil current and magnetic flux density at the center. (d) Cyclic electrical responsiveness under different magnetic fields. (e) Curves of magnetic flux density at the center and the corresponding responsive deviation/deflection angle of the SMAF sample. (f) Single-cycle curves of the applied magnetic field and the electrical sensing signals of SMAF. The response and reset times are marked.

gradually adding weights, the relationship of the loading-magnetic flux density-lifting obliquity was obtained, shown in Figure 3b. Then, the specific lifting obliquity and the corresponding applied magnetic flux density and torque per MAF unit mass were taken and fitted. It can be seen in Figure 3c that there is a linear relationship of torque per MAF unit mass and the strength of horizontal magnetic field for a specific lifting obliquity. Here, the slope represents the torque per unit mass of MAF per unit field. When the MAF sample with magnetic chains oriented lengthwise was oriented at the angle of approximately 40°, the torque per unit MAF mass per unit field is 11.4 Nm/kg T. In addition, the weight-loading experiments were conducted for the MAF sample with magnetic chains oriented breadthwise (MAF-90°). It is observed that the MAF sample is twisted in the direction of cutting magnetic line (Figure 3a,d). The relationship between torsion angle, applied magnetic field, and the added weights are demonstrated in Figure 3e. Hereby, the torsion angle is defined as the angle between the free short edge of the strip-shaped sample and the horizontal magnetic field. Under the same magnetic field, MAF-90° sample with different loads has almost the same magnetoinduced torsion angles. The stability of MAF with magnetic chains oriented lengthwise is also explored and presented in Figure S4 and Movie S1. Clearly, the magnetism actuation shows no degradation after 10 000 cyclic excitations, indicating good reversibility and durability of MAF.

Moreover, MAF samples with different magnetic chain orientations were prepared with the crossing angle (θ) between the magnetic chain and the long edge varying from 0 to 90°. The experiment settings are the same as those described in the weight-loading experiment. Driven by magnetic-field-induced force, MAF samples were twisted into different states (Figure 3d). Due to mechanical constraints, the unilaterally structured MAF samples were biased toward the grating direction when a horizontal magnetic field was applied. Figure 3d,f shows that the torsion angle and the lifting obliquity of MAF strips with different magnetic chain orientations are different under the same magnetism actuation. In Figure 3d, the left optical images were taken without a magnetic field and the right ones were under 0.130 T horizontal field. For MAF-75°, the applied magnetic flux density is 0, 0.027, 0.036, and 0.130 T, respectively. Especially, it can be observed that 45° is the dividing line. For a MAF with a crossing angle of 45° or less, as the magnetism increased, the induced torsion angle and the lifting obliquity gradually increased. However, for a MAF with a larger crossing angle, there is a short lifting segment at low fields while the lift retracted at high fields. This phenomenon may provide new ideas for the special design of soft robots.

Self-Sensing. To better characterize the magnetic−mechanic−electric coupling characteristics of SMAF, the electrical changes under mechanical load were first evaluated. Figure 4a exhibits the measurement system, which consists of four parts: a reciprocating drive, a hertz regulator, a home-made sample holder, an electrical property test system (Modulab MTS), and a data storage analyzing system (software). As depicted in Figure 4a, the SMAF sample with magnetic chains oriented lengthwise was pasted on a holder, and the grating side of the sample is the adhered surface. Apply and change the deflection stimuli via adjusting the distance between reciprocating drive and the holder and adjust the loading frequencies through a hertz regulator. Figure 4b shows the relative resistance change $\Delta R/R$ depending on the applied deflection of up to 8.0 mm when the drive rod was loaded from direction I, where R is the initial electrical resistance and ΔR is the resistance variation. With an increase in deflection, the bending angles of SMAF toward the grating side increased, and the absolute value of the peak value of normalized resistance

https://dx.doi.org/10.1021/acsami.1c01721
ACS Appl. Mater. Interfaces 2021, 13, 13724−13734

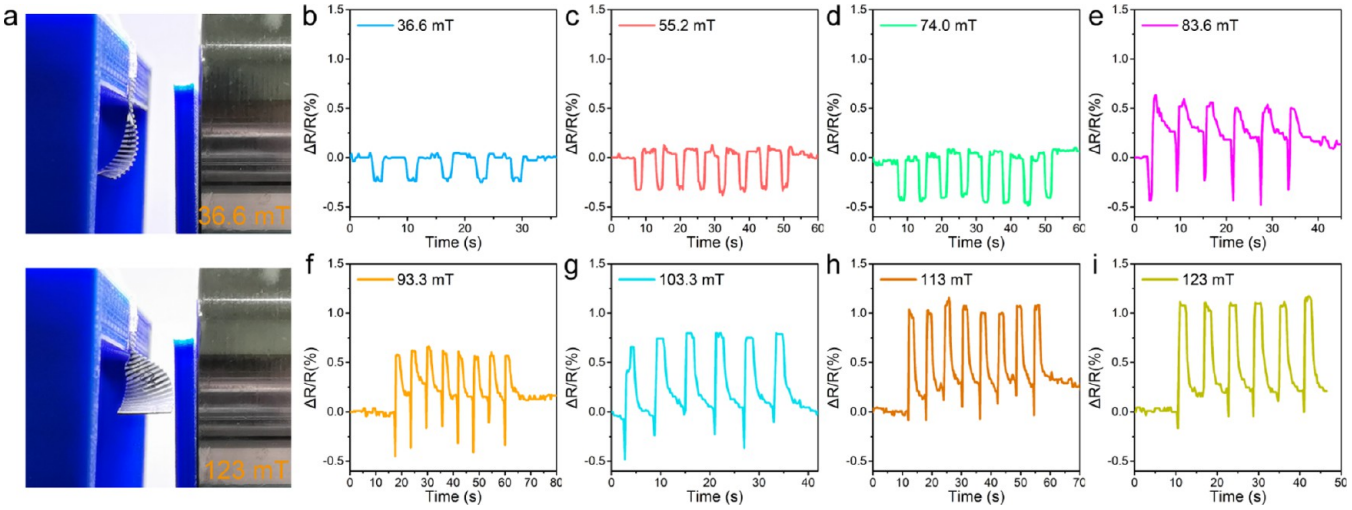

Figure 6. Magnetism sensing property of sample SMAF with magnetic chains oriented breadthwise. (a) Optical images of the bending deformation of sample SMAF under the self-fabricated electromagnetic testing system devices. The sample was fixed on a holder. (b–i) Variation of $\Delta R/R$ of SMAF as a function of magnetic flux density in cycles.

variation increased correspondingly, indicating that electrical performance is distinctly dependent on the curled angle (Figure 4c). The electrical responses were maintained well for different deflection stimuli and reproducible under multiple tests. Moreover, the influence of the applied frequency/rates on the tendency and peak value of normalized resistance variation was tested. Figure 4d demonstrated that the applied frequency had no significant influence on the electrical property in a certain range (0.1–1.0 Hz). In addition, as displayed in Figure 4e, SMAF had an approximately −4.5% increment in resistance and exhibited good stability, recoverability, and repeatability under continuous cyclic loading (1.5 mm deflection).

Then, the electric responsiveness of SMAF is investigated when the drive rod is loaded from direction II. As exhibited in Figure 4f, when the load came from direction II, the electrical resistance variation was positive, opposite to that shown in Figure 4b. This is because the as-prepared SMAF sample is unilateral, and the thickness of the front and back layers of the AgNW sensing layer are different. When the SMAF sample is bent in different directions, the AgNW sensing layer presents two different states: one is in a compressed state and the other is in a stretched state. Therefore, when the drive rod was loaded from direction I and direction II, the electrical changes are negative and positive values, respectively. Such a result will be propitious to the distinction of actuation direction. This helps distinguish changes. Also, when the frequency was set from 0.25 to 1.0 Hz, the loading frequency/speed of mechanical stimuli does not affect the sensing behavior of SMAF (Figure 4g). Figure 4h exhibits the real-time monitoring of the normalized relative resistance in the cycled loading and unloading of drive rod from direction II, indicating the excellent durability of the mechanical–electrical responses.

In addition to evaluating the sensitivity to mechanical stimuli, the electrical response of SMAF to magnetic field excitation was also systematically tested. The SMAF sample with a length of 15 mm and a width of 10 mm was immobilized on the home-made holder. Then, the sample and the holder were placed in the middle of two facing electromagnets shown in Figure 5a. By adjusting the electromagnetic coil current by means of a DC power supply (the currents of two electromagnets were reversed), an almost uniform magnetic field was applied at the distance between the two electromagnets. When the current was set to 1 A, the simulation result of the magnetic field distribution between electromagnets is shown in Figure 5b. Also, Figure 5c demonstrates the relationship between the coil current and the magnetic flux density at the center of the electromagnetic system. As the applied current was set as 0.25, 0.3, 0.35, 0.4, 0.5, 0.55, and 0.6 A (square wave), the corresponding magnetic flux density was 22.2, 27.4, 31.9, 36.6, 46.0, 51.5, and 55.2 mT, respectively, and the average normalized resistance variation of SMAF was −0.46, −0.52, −0.54, −1.8, −2.6, −4.2, and −4.8%, respectively (Figure 5d). It can be clearly seen that for the same magnetic density interval, the relative change in resistance under a high field is greater than that under a low field (Figure 5d), which is consistent with the observed bending deformation of the sample. Figure 5e exhibits the applied transient magnetic field and the corresponding responsive deviation/deflection angle curve of the SMAF sample. The bending deformation response curve and the magnetic field curve almost coincide, and the lag time was only about 10 ms. When the magnetic field was removed, the sample returned to its original state. Figure 5f shows the single-cycle curve of magnetic flux density vs time and the curve of the output normalized resistance variation vs time. Also, the electrical sensing signal of the sample is slightly delayed in the magnetic field response. The response and reset times of the SMAF sample were approximately 60 and 80 ms, respectively (including the response and reset times of magnetic field) as marked in Figure 5f. The above results show that SMAF has a rapid and stable mechanical and electrical response, ensuring the outstanding actuation and self-sensing performance of the designed actuator and soft robot.

The SMAF sample with magnetic chains oriented breadthwise underwent a twist in the direction of the cutting magnetic induction line. Under low field, SMAF had a negative resistance change. As displayed in Figure 6a, the deformation of SMAF had a dominant inward bending when the applied magnetic field was 36.6 mT. Here, we refer to the bending in the direction away from the magnetic grating as inward bending. Conversely, the bending toward the magnetic grating

https://dx.doi.org/10.1021/acsami.1c01721
ACS Appl. Mater. Interfaces 2021, 13, 13724–13734

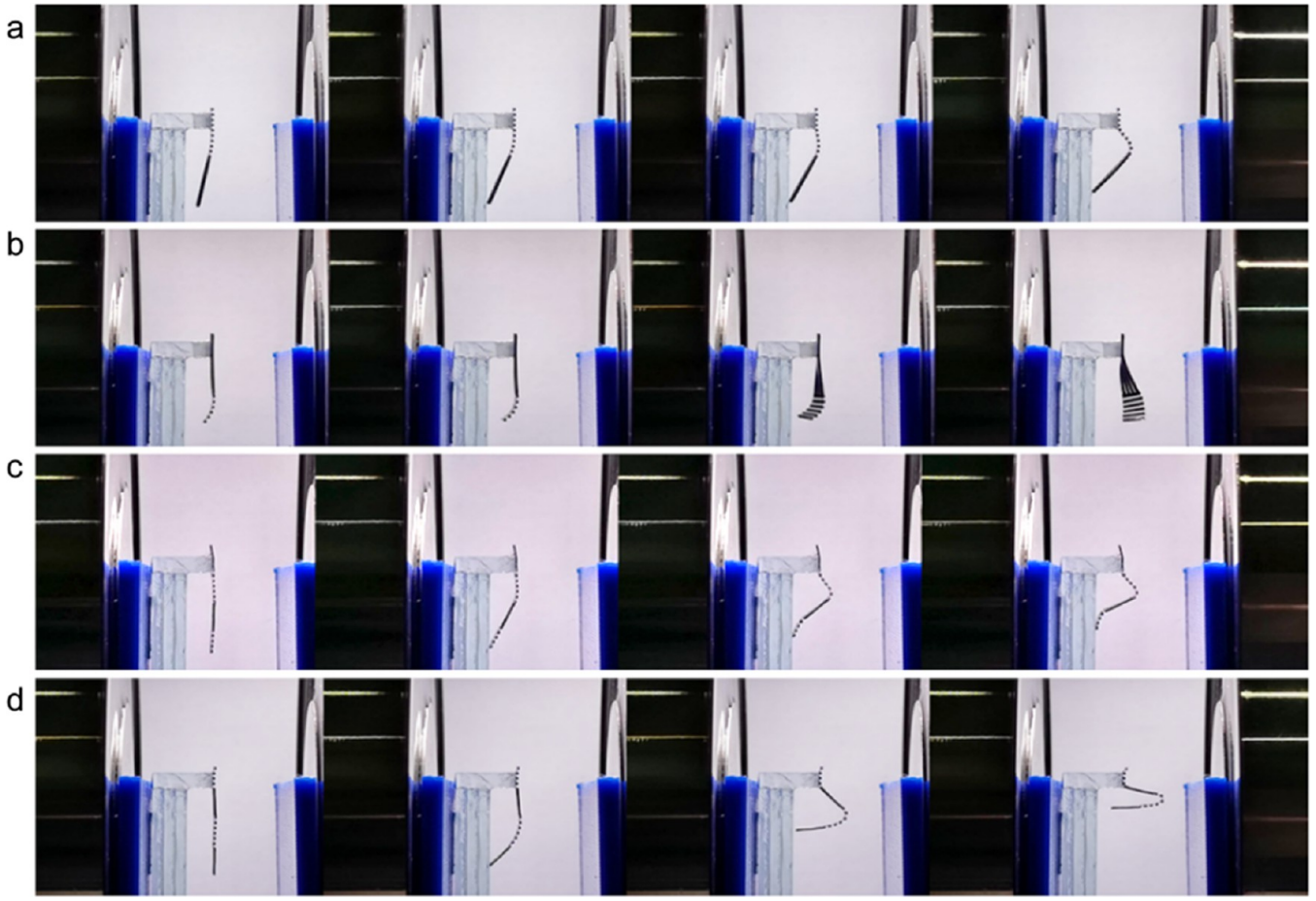

Figure 7. Deformation of the MAF samples with different magnetic orientation combinations under different magnetic fields. (a) MAF with cross-angles of 90 and 0° in a ratio of 1:2 that was bent double gradually when the magnetic flux density increased. (b) Deflected and warped MAF with cross-angles of 0 and 90° in a ratio of 2:1. (c) MAF with cross-angles of 90, 0, and 90° in a ratio of 1:1:1 that gradually folded up like an inchworm. (d) MAF with cross-angles of 0, 90, and 0° in a ratio of 1:1:1 that can gradually fold to look like a praying mantis's raised forearm when the magnetic field is applied.

is called outward bending. Under a high field, the resistance presented a trend of first decline and then rise, and the ultimate resistance change was positive, representing that the initial shape change of SMAF is mainly inward bending, and the increase in resistance with the increase of transient magnetic field strength was caused by outward bending deformation gradually occupying the predominant position. Such results show that SMAF can not only discriminate bending actuation in different directions but also distinguish bending and torsion actuation modes to a certain extent. It means SMAF has the enticing application potential in self-monitoring actuators.

Multifunctional Shape Manipulation. For the magnetic strips that are pinned at one end, the magnetic force brings the chains closer to alignment with the field. We know that under the excitation of the as-described field in the magnetism-responsive deformation section, MAF-0° was deformed in a bended mode and MAF-90° was deformed in a torsional mode. Structures with other crossing angles yield a combined bending and torsion (Figure 3). The MAF samples with a structure containing both parallel and normal magnetization components were prepared, verifying that advanced magnetism-induced deformation can be achieved by combining the design rules together. Magnetics fields of 0, 27.4, 55.2, 83.6, and 113 mT were applied to the samples in a sequence, as displayed in Figure 7a–d. MAF with cross-angles of 90 and 0° in a ratio of 1:2 was bent double gradually when the magnetic flux density increased (Figure 7a). MAF with cross-angles of 0 and 90° in a ratio of 2:1 deflected and warped under the field (Figure 7b). MAF with cross-angles of 90, 0, and 90° in a ratio of 1:1:1 gradually folded up like an inchworm with an increase in field strength (Figure 7c). Moreover, in Figure 7d, the crossing angles of the MAF sample are 0, 90, and 0°, and the ratio is 1:1:1. When a magnetic field was applied, it gradually folded like a mantis's raising forearm. Naturally more bionic actuation functions can be produced by designing a magnetic orientation combination structure.

The deformation of MAF under a magnetic field is not straightforwardly attributable to the magnetic chain distribution. Also, the overall structure and the applied magnetic field distribution affects the deformation. As shown in Figure 8, the unilaterally structured MAF with different shapes was fabricated and the actuation was investigated in magnetic field gradients generated by a single electromagnet. Here, the shaped MAF samples were entirely made of magneto-rheological elastomer without a nonmagnetic part in Figure 8a–c. Figure S5 exhibits the field distribution and the relationship between coil current and magnetic flux density at the center and at the edge. The samples were placed in the axis of an electromagnet. Displayed in Figure 8a, the spindle-

https://dx.doi.org/10.1021/acsami.1c01721
ACS Appl. Mater. Interfaces 2021, 13, 13724–13734

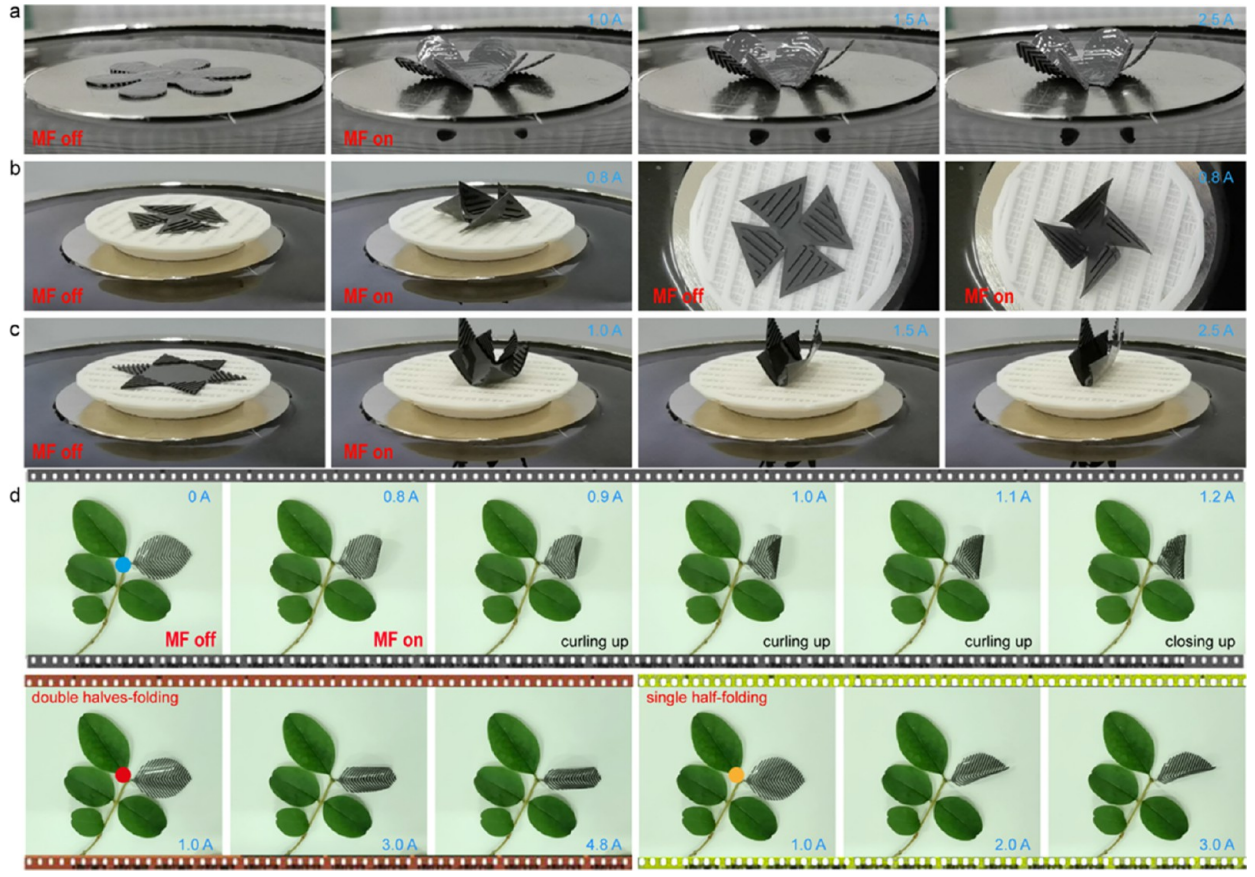

Figure 8. Shape-programmable magnetoactive composite materials that exhibit integrated multifunctional shape manipulations. (a) Flowerlike MAF sample lifted with the increasing electromagnet coil currents. (b) MAF sample that was self-assembled to a smart windmill under contactless stimuli. (c) Hexagram MAF sample that closed its leaves like a Venus Flytrap. (d) A demonstration of a smart leaf that had various folding behaviors under different magnetic fields.

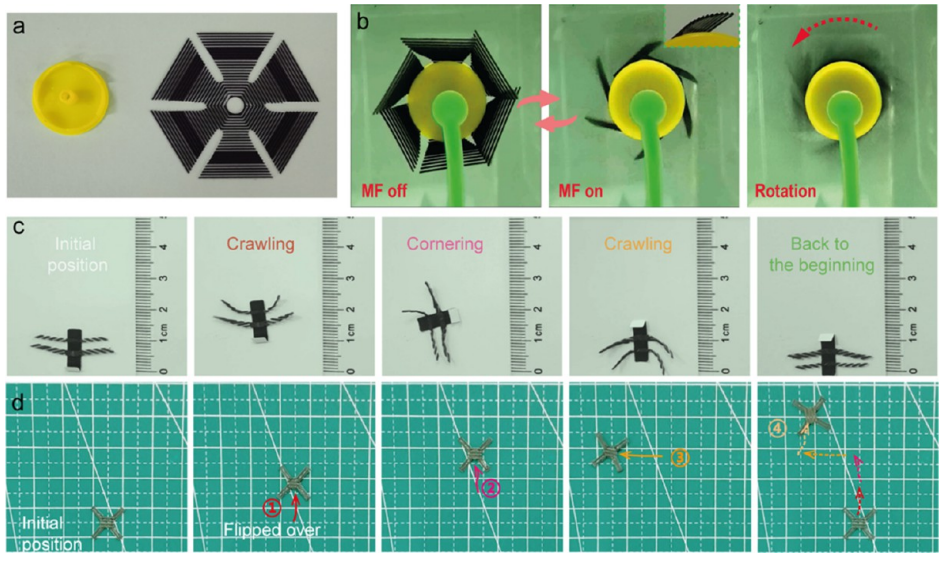

Figure 9. Assembled device of magnetoactive composites. (a, b) Photographs of the assembly and response of magnetism-responsive windmills. (c) Crawling polypod-like soft minirobot based on MAF. (d) Proof-of-concept soft minirobot that can be moved by flipping.

shaped petals of flowerlike MAF sample were magnetically oriented in a vein distribution and their free ends were lifted with the increasing electromagnet coil current. It can be clearly seen that bending dominates in the deformation. The MAF sample with a triangular configuration was self-assembled to a smart windmill under the contactless magnetic stimuli (Figure 8b and Movie S2). Also shown in Figure 8c, the hexagram MAF sample closed its leaves like a Venus Flytrap (Movie S3). The magnetic chains orientation of the blades of both smart windmill and star-shaped MAF are perpendicular to one side of

https://dx.doi.org/10.1021/acsami.1c01721
ACS Appl. Mater. Interfaces 2021, 13, 13724−13734

the triangle. The twisting of the windmill blades was very obvious, whereas bending deformation of the star-shaped MAF blades played an absolute dominant role.

In addition, a smart leaf made of MAF was prepared to investigate the possible actuation modes under different magnetic fields (Movie S4). The smart leaf was modeled like real leaves, and its veins are full of magnetic particles. Figure S5 exhibits the precise positions of a smart leaf in the same gradient magnetic field. Under the action of a magnetic field, the leaf had a variety of actuation behaviors, such as curling up, folding both halves, and folding single half (Figure 8d). Regarding the double halves-folding mode, it is like a Venus Flytrap without bristles. That is, when the noncontact environmental magnetic field was turned on, the two halves of the leaf abut each other with the middle rib as the axis. The results demonstrate that the shape-programmable magnetoactive composite materials can exhibit integrated multifunctional shape manipulations.

Besides the actuation modes such as opening, closing, and curling, it is also possible to develop motion-driven modes through combinations. As shown in Figure 9a, taking advantage of this orientation-defined deformation, we prepared a complex MAF sample composed of triangular films with the same grating orientation and assembled it with a shaft (Figure 9a). Interestingly, when a magnetic field was applied, it deformed into a windmill and the wind rotated it (Figure 9b and Movie S5). Moreover, after the sensing layer was coated on the blade, we could monitor the states of the windmill blade through the output electrical signal (Figure S6). Figure 9c shows a crawling polypod-like soft minirobot based on MAF. Under the changed magnetic field, the soft-structure minirobot was remotely controlled to crawl forward and spot turn without contact (Movie S6). Additionally, in the preparation processes, if we replace the soft magnetic particles with hard magnetic particles and apply a magnetic field for magnetization during the vulcanization process, MAF becomes magnetic. The as-prepared minirobot flipped to move forward or turn under the excitation by an alternating magnetic field (Figure 9d and Movie S7). Ingeniously combining the hard magnetic particle filling part and the soft magnetic particle filling part together may produce actuators with smart actuation modes. This is a challenge in analyzing the distribution of micromagnets and soft magnetic particles and controlling the magnetic field. All of the demo samples in the present study are simple proof-of-concept minirobots and no further attempts were made to develop more complex MAF samples due to the lack of equipment to flexibly control the external magnetic field. We envision that this research provides a new manufacturing method of magnetoactive composite toward self-sensing actuator and soft robotics, which is conducive to the exploration of mechanic−magnetic−electric coupling mechanism, and based on the design concepts presented in the paper, more interesting and complicated actuation can be achieved.

CONCLUSIONS

In summary, a variety of planar magnetoactive composites at the millimeter scale were prepared using cost-effective mask-patterning and spin coating technology. In this method, the soft magnetic carbonyl iron particles and conductive silver nanowires were precisely oriented and patterned without a magnetic field generator or other expensive devices. The as-fabricated SMAF samples exhibited the advantages of excellent flexibility, multiple actuation modes, outstanding self-monitoring, ultrahigh response time, and good stability. SMAF can not only discriminate bending actuation in different directions but also distinguish bending and torsion actuation modes to a certain extent. The electrical response and reset times of the SMAF sample were approximately 60 and 80 ms, respectively, which contained the response and reset times of magnetic field. Besides, the shape-programmable magnetoactive composites showed integrated multifunctional shape manipulations under different magnetic fields. These results demonstrate that the as-prepared self-sensing magnetism-responsive anisotropic composite is an enticing and promising candidate to expand the application range of the future intelligent actuating system.

EXPERIMENTAL SECTION

Materials. The poly(dimethylsiloxane) precursor and curing agent (Sylgard 184) were purchased from Dow Corning GmbH. The carbonyl iron particles (CN-type) were purchased from BASF Aktiengesellschaft, Germany. The particle size range is 1−17 μm, and the median diameter is about 7 μm. The poly(dimethylsiloxane) (PDMS) precursor and curing agent (Sylgard 184) were supplied from Dow Corning GmbH. Reagents (analytical grade purity) for the fabrication of AgNWs were purchased from Sinopharm Chemical Reagent Co. Ltd., Shanghai, China, and used without further purification.

Fabrication of AgNWs. AgNWs are conductive components of the sensing unit and prepared successfully by a simple synthesis method.[41] Poly(vinylpyrrolidone) powder (5.86 g) with a molecular weight of about 40 000 was added to 190 mL of glycerin at 90 °C and stirred until the powder was completely dissolved in the glycerin. The mixed solution was then cooled to 50 °C, and 1.58 g of silver nitrate powder was added. Deionized water (0.5 mL), 59 mg of sodium chloride, and 10 mL of glycerin were weighed and added to the mixed solution. Then, the above reaction solution was heated to 210 °C. After that, the heating was stopped, the solution was immediately transferred to a beaker, and a total of 200 mL of deionized water was added several times. After allowing the reactant to stand for several days, the supernatant was poured out and then the remaining reactant suspension was washed with deionized water several times to obtain an aqueous dispersion of silver nanowires.

SMAF Fabrication. The PDMS prepolymer with a curing agent (10:1 by weight) and carbonyl iron particles (60 wt %) were mixed by stirring for 10 min. Then, the mixture was poured onto a structured master mold, which was printed by a fused deposition printer (Creator-pro, FlashForge Technology Co., Ltd., China) or a light-curing printer (MiiCraft 125, Rays Optics Technology Co., Ltd., China), spin-coated at 500 rpm for 60 s, and cured at 90 °C for 20 min. After scraping off the excess magnetorheological elastomer at the protrusion of master mold, the PDMS prepolymer (10:1 curing ratio) was poured at the surface of the mold, spin-coated at 1250 rpm for 60 s, and cured at 90 °C for 20 min. Then, the reusable masking film was attached to the cured PDMS film. Here, the reusable masking films with a snake-shaped pattern were obtained by hollowing out a commercially available 10 micron thick poly(ethylene terephthalate) film via laser cutting technology. The paths of the pattern were coated with 0.04 mL of an aqueous solution of AgNWs (concentration: 7 mg/mL) and dried in the air for 10 min. This coating operation was repeated five times to form a conductive AgNW network and then the masking film was peeled off. The wires were adhered to the electrode zones of the conductive pattern by a silver paste. After that, the PDMS prepolymer was poured on the surface by spin coating at 1000 rpm for 60 s to completely cover the paths, and they were cured at 90 °C for 20 min. The resulting self-sensing magnetism-responsive anisotropic film was released by manual peeling (Figure 1). The preparation method of MAF is similar to that of SMAF, except that the AgNW sensing layer coating operations are not performed.

Characterization. The microstructures were characterized by a 3D optical microscope (Olympus DSX510) and scanning electron microscopy (SEM, Gemini 500, Carl Zeiss, Jena, Germany). The

https://dx.doi.org/10.1021/acsami.1c01721
ACS Appl. Mater. Interfaces 2021, 13, 13724−13734

hysteresis loops of the materials were tested by HyMDC (Hysteresis Measurement of Soft and Hard Magnetic Materials). The magnetic field was afforded by Magnetic Power Systems (XDA-120/70, Yueqing Xingda Electric Co., Ltd., China) by adjusting the electromagnetic coil current by means of a DC power supply (ITECH IT6724). The magnetic flux density was measured by a digital teslameter (HT20, Shanghai Hengtong Magnetic Technology Co., Ltd., China). The electrical properties were measured by a Modulab material test system (Solartron Analytical, AMETEK Advanced Measurement Technology, Inc., U.K.). The magnetism-responsive anisotropic film was cut into ribbons (15×3.5 mm^2) for bending tests and ribbons (15×10 mm^2) for electrical properties measuring tests. All of the measurements were conducted in the air at room temperature (25 °C).

■ ASSOCIATED CONTENT

Supporting Information

The Supporting Information is available free of charge at https://pubs.acs.org/doi/10.1021/acsami.1c01721.

Microstructure of the designed AgNW sensing layer (unit of length: mm); the prepared magnetism-responsive anisotropic films; vibrating sample magnetometer (VSM) data measured perpendicular and parallel to magnetic chains with the MAF samples shown in Figure 2b at room temperature; the single electromagnet and the applied magnetic field distribution when the coil current is set as 1 A; long-term working stability of magnetism-responsive anisotropic ribbons with magnetic chains oriented lengthwise ($15 \times 5 \times 0.5$ mm^3) under the magnetic flux density of 60 mT; the relationship between the coil current and magnetic flux density at the green cross-points remarked in Figure S5a; and the output relative electrical resistance variations of the magnetism-responsive windmill (PDF)

Movie S1 (MP4)
Movie S2 (MP4)
Movie S3 (MP4)
Movie S4 (MP4)
Movie S5 (MP4)
Movie S6 (MP4)
Movie S7 (MP4)

■ AUTHOR INFORMATION

Corresponding Authors

Xinglong Gong − *CAS Key Laboratory of Mechanical Behavior and Design of Materials, Department of Modern Mechanics, CAS Center for Excellence in Complex System Mechanics, University of Science and Technology of China (USTC), Hefei 230027, China;* orcid.org/0000-0001-6997-9526; Email: gongxl@ustc.edu.cn

Dongsheng Zhang − *Shanghai Institute of Applied Mathematics and Mechanics, School of Mechanics and Engineering Science, Shanghai University, Shanghai 200444, China; Shanghai Key Laboratory of Mechanics in Energy Engineering, Shanghai 200072, China*; Email: donzhang@staff.shu.edu.cn

Authors

Li Ding − *Shanghai Institute of Applied Mathematics and Mechanics, School of Mechanics and Engineering Science, Shanghai University, Shanghai 200444, China; Shanghai Key Laboratory of Mechanics in Energy Engineering, Shanghai 200072, China;* orcid.org/0000-0001-7883-9103

Jingyi Zhang − *CAS Key Laboratory of Mechanical Behavior and Design of Materials, Department of Modern Mechanics, CAS Center for Excellence in Complex System Mechanics, University of Science and Technology of China (USTC), Hefei 230027, China*

Quan Shu − *CAS Key Laboratory of Mechanical Behavior and Design of Materials, Department of Modern Mechanics, CAS Center for Excellence in Complex System Mechanics, University of Science and Technology of China (USTC), Hefei 230027, China*

Siyong Liu − *Shanghai Institute of Applied Mathematics and Mechanics, School of Mechanics and Engineering Science, Shanghai University, Shanghai 200444, China; Shanghai Key Laboratory of Mechanics in Energy Engineering, Shanghai 200072, China*

Shouhu Xuan − *CAS Key Laboratory of Mechanical Behavior and Design of Materials, Department of Modern Mechanics, CAS Center for Excellence in Complex System Mechanics, University of Science and Technology of China (USTC), Hefei 230027, China;* orcid.org/0000-0002-8232-9736

Complete contact information is available at: https://pubs.acs.org/10.1021/acsami.1c01721

Notes

The authors declare no competing financial interest.

■ ACKNOWLEDGMENTS

Financial supports from the National Key R&D Program of China (2018YFF01014200) and the National Natural Science Foundation of China (Grant Nos. 11822209, 11872240, 11972032, and 12072338) are gratefully acknowledged. This work was partially carried out at the USTC Center for Micro- and Nanoscale Research and Fabrication.

■ ABBREVIATIONS

SMAF, self-sensing magnetism-responsive anisotropic film
PDMS, poly(dimethylsiloxane)
AgNW, silver nanowire
MAF, magnetism-responsive anisotropic film
CIP, carbonyl iron particle
SEM, scanning electron microscope
R, initial electrical resistance
ΔR, resistance variation

■ REFERENCES

(1) Miriyev, A.; Stack, K.; Lipson, H. Soft Material for Soft Actuators. *Nat. Commun.* **2017**, *8*, No. 596.
(2) Hines, L.; Petersen, K.; Lum, G. Z.; Sitti, M. Soft Actuators for Small-Scale Robotics. *Adv. Mater.* **2017**, *29*, No. 1603483.
(3) Chorsi, M. T.; Curry, E. J.; Chorsi, H. T.; Das, R.; Baroody, J.; Purohit, P. K.; Ilies, H.; Nguyen, T. D. Piezoelectric Biomaterials for Sensors and Actuators. *Adv. Mater.* **2019**, *31*, No. 1802084.
(4) de Rivaz, S. D.; Goldberg, B.; Doshi, N.; Jayaram, K.; Zhou, J.; Wood, R. J. Inverted and Vertical Climbing of a Quadrupedal Microrobot Using Electroadhesion. *Sci. Rob.* **2018**, *3*, No. eaau3038.
(5) Guan, Q. H.; Sun, J.; Liu, Y. J.; Wereley, N. M.; Leng, J. S. Novel Bending and Helical Extensile/Contractile Pneumatic Artificial Muscles Inspired by Elephant Trunk. *Soft Rob.* **2020**, *7*, 597−614.
(6) Löwenberg, C.; Balk, M.; Wischke, C.; Behl, M.; Lendlein, A. Shape-Memory Hydrogels: Evolution of Structural Principles to Enable Shape Switching of Hydrophilic Polymer Networks. *Acc. Chem. Res.* **2017**, *50*, 723−732.
(7) Zhang, Y.-L.; Liu, Y.-Q.; Han, D.-D.; Ma, J.-N.; Wang, D.; Li, X.-B.; Sun, H.-B. Quantum-Confined-Superfluidics-Enabled Moisture

Actuation Based on Unilaterally Structured Graphene Oxide Papers. *Adv. Mater.* **2019**, *31*, No. 1901585.
(8) Zhao, R.; Kim, Y.; Chester, S. A.; Sharma, P.; Zhao, X. Mechanics of Hard-Magnetic Soft Materials. *J. Mech. Phys. Solids* **2019**, *124*, 244−263.
(9) Tang, S.; Zhang, X.; Sun, S.; Yuan, D.; Zhao, Q.; Yan, S.; Deng, L.; Yun, G.; Zhang, J.; Zhang, S.; Li, W. Versatile Microfluidic Platforms Enabled by Novel Magnetorheological Elastomer Microactuators. *Adv. Funct. Mater.* **2018**, *28*, No. 1705484.
(10) Huang, H.-W.; Sakar, M. S.; Petruska, A. J.; Pané, S.; Nelson, B. J. Soft Micromachines with Programmable Motility and Morphology. *Nat. Commun.* **2016**, *7*, No. 12263.
(11) Lum, G. Z.; Ye, Z.; Dong, X.; Marvi, H.; Erin, O.; Hu, W.; Sitti, M. Shape-Programmable Magnetic Soft Matter. *Proc. Natl. Acad. Sci. U.S.A.* **2016**, *113*, E6007−E6015.
(12) Shu, J.; Tang, S.-Y.; Zhao, S.; Feng, Z.; Chen, H.; Li, X.; Li, W.; Zhang, S. Rotation of Liquid Metal Droplets Solely Driven by the Action of Magnetic Fields. *Appl. Sci.* **2019**, *9*, No. 1421.
(13) Morales, D.; Bharti, B.; Dickey, M. D.; Velev, O. D. Bending of Responsive Hydrogel Sheets Guided by Field-Assembled Microparticle Endoskeleton Structures. *Small* **2016**, *12*, 2283−2290.
(14) Gao, W.; Wang, L.; Wang, X.; Liu, H. Magnetic Driving Flowerlike Soft Platform: Biomimetic Fabrication and External Regulation. *ACS Appl. Mater. Interfaces* **2016**, *8*, 14182−14189.
(15) Jeon, J.; Park, J. E.; Park, S. J.; Won, S.; Zhao, H. B.; Kim, S.; Shim, B. S.; Urbas, A.; Hart, A. J.; Ku, Z.; Wie, J. J. Shape-Programmed Fabrication and Actuation of Magnetically Active Micropost Arrays. *ACS Appl. Mater. Interfaces* **2020**, *12*, 17113−17120.
(16) Goc, K.; Gaska, K.; Klimczyk, K.; Wujek, A.; Prendota, W.; Jarosinski, L.; Rybak, A.; Kmita, G.; Kapusta, C. Influence of Magnetic Field-Aided Filler Orientation on Structure and Transport Properties of Ferrite Filled Composites. *J. Magn. Magn. Mater.* **2016**, *419*, 345−353.
(17) Qiao, X.; Lu, X.; Gong, X.; Yang, T.; Sun, K.; Chen, X. Effect of Carbonyl Iron Concentration and Processing Conditions on the Structure and Properties of the Thermoplastic Magnetorheological Elastomer Composites Based on Poly(Styrene-B-Ethylene-Co-Butylene-B-Styrene) (Sebs). *Polym. Test.* **2015**, *47*, 51−58.
(18) Schmauch, M. M.; Mishra, S. R.; Evans, B. A.; Velevt, O. D.; Tracy, J. B. Chained Iron Microparticles for Directionally Controlled Actuation of Soft Robots. *ACS Appl. Mater. Interfaces* **2017**, *9*, 11895−11901.
(19) Zhang, J.; Pang, H.; Wang, Y.; Gong, X. The Magneto-Mechanical Properties of Off-Axis Anisotropic Magnetorheological Elastomers. *Compos. Sci. Technol.* **2020**, *191*, No. 108079.
(20) Liu, J. A. C.; Gillen, J. H.; Mishra, S. R.; Evans, B. A.; Tracy, J. B. Photothermally and Magnetically Controlled Reconfiguration of Polymer Composites for Soft Robotics. *Sci. Adv.* **2019**, *5*, No. eaaw2897.
(21) Xu, T.; Zhang, J.; Salehizadeh, M.; Onaizah, O.; Diller, E. Millimeter-Scale Flexible Robots with Programmable Three-Dimensional Magnetization and Motions. *Sci. Rob.* **2019**, *4*, No. eaav4494.
(22) Kokkinis, D.; Schaffner, M.; Studart, A. R. Multimaterial Magnetically Assisted 3d Printing of Composite Materials. *Nat. Commun.* **2015**, *6*, No. 8643.
(23) Kim, Y.; Yuk, H.; Zhao, R. K.; Chester, S. A.; Zhao, X. H. Printing Ferromagnetic Domains for Untethered Fast-Transforming Soft Materials. *Nature* **2018**, *558*, 274−279.
(24) Qi, S.; Guo, H.; Fu, J.; Xie, Y.; Zhu, M.; Yu, M. 3d Printed Shape-Programmable Magneto-Active Soft Matter for Biomimetic Applications. *Compos. Sci. Technol.* **2020**, *188*, No. 107973.
(25) Nguyen, V. Q.; Ahmed, A. S.; Ramanujan, R. V. Morphing Soft Magnetic Composites. *Adv. Mater.* **2012**, *24*, 4041−4054.
(26) Lin, Z. H.; Fan, X. J.; Sun, M. M.; Gao, C. Y.; He, Q.; Xie, H. Magnetically Actuated Peanut Colloid Motors for Cell Manipulation and Patterning. *ACS Nano* **2018**, *12*, 2539−2545.
(27) Choi, D. S.; Kim, T. H.; Lee, S. H.; Pang, C.; Bae, J. W.; Kim, S. Y. Beyond Human Hand: Shape-Adaptive and Reversible Magneto-rheological Elastomer-Based Robot Gripper Skin. *ACS Appl. Mater. Interfaces* **2020**, *12*, 44147−44155.
(28) Kang, J.-H.; Kim, H.; Santangelo, C. D.; Hayward, R. C. Enabling Robust Self-Folding Origami by Pre-Biasing Vertex Buckling Direction. *Adv. Mater.* **2019**, *31*, No. 0193006.
(29) Becker, K. P.; Chen, Y.; Wood, R. J. Mechanically Programmable Dip Molding of High Aspect Ratio Soft Actuator Arrays. *Adv. Funct. Mater.* **2020**, *30*, No. 1908919.
(30) Gu, G.; Zou, J.; Zhao, R.; Zhao, X.; Zhu, X. Soft Wall-Climbing Robots. *Sci. Rob.* **2018**, *3*, No. eaat2874.
(31) Chen, D.; Liu, Q.; Han, Z.; Zhang, J.; Song, H.; Wang, K.; Song, Z.; Wen, S.; Zhou, Y.; Yan, C.; Shi, Y. 4d Printing Strain Self-Sensing and Temperature Self-Sensing Integrated Sensor-Actuator with Bioinspired Gradient Gaps. *Adv. Sci.* **2020**, *7*, No. 2000584.
(32) Kim, S. Y.; Choo, Y.; Bilodeau, R. A.; Yuen, M. C.; Kaufman, G.; Shah, D. S.; Osuji, C. O.; Kramer-Bottiglio, R. Sustainable Manufacturing of Sensors onto Soft Systems Using Self-Coagulating Conductive Pickering Emulsions. *Sci. Rob.* **2020**, *5*, No. eaay3604.
(33) Luo, M.; Skorina, E. H.; Tao, W. J.; Chen, F. C.; Ozel, S.; Sun, Y. N.; Onal, C. D. Toward Modular Soft Robotics: Proprioceptive Curvature Sensing and Sliding-Mode Control of Soft Bidirectional Bending Modules. *Soft Rob.* **2017**, *4*, 117−125.
(34) Kim, Y.; Parada, G. A.; Liu, S.; Zhao, X. Ferromagnetic Soft Continuum Robots. *Sci. Rob.* **2019**, *4*, No. eaax7329.
(35) Kuo, J. C.; Huang, H. W.; Tung, S. W.; Yang, Y. J. A Hydrogel-Based Intravascular Microgripper Manipulated Using Magnetic Fields. *Sens. Actuators, A* **2014**, *211*, 121−130.
(36) Feng, J. B.; Xuan, S. H.; Ding, L.; Gong, X. L. Magnetoactive Elastomer/Pvdf Composite Film Based Magnetically Controllable Actuator with Real-Time Deformation Feedback Property. *Composites, Part A* **2017**, *103*, 25−34.
(37) Liu, S.; Wang, S.; Xuan, S.; Zhang, S.; Fan, X.; Jiang, H.; Song, P.; Gong, X. Highly Flexible Multilayered E-Skins for Thermal-Magnetic-Mechanical Triple Sensors and Intelligent Grippers. *ACS Appl. Mater. Interfaces* **2020**, *12*, 15675−15685.
(38) Zheng, W.; Razal, J. M.; Whitten, P. G.; Ovalle-Robles, R.; Wallace, G. G.; Baughman, R. H.; Spinks, G. M. Artificial Muscles Based on Polypyrrole/Carbon Nanotube Laminates. *Adv. Mater.* **2011**, *23*, 2966−2970.
(39) Aliev, A. E.; Oh, J.; Kozlov, M. E.; Kuznetsov, A. A.; Fang, S.; Fonseca, A. F.; Ovalle, R.; Lima, M. D.; Haque, M. H.; Gartstein, Y. N.; et al. Giant-Stroke, Superelastic Carbon Nanotube Aerogel Muscles. *Science* **2009**, *323*, 1575−1578.
(40) Phan, H.-P.; Dinh, T.; Nguyen, T. K.; Vatani, A.; Riduan, A.; et al. Self-Sensing Paper-Based Actuators Employing Ferromagnetic Nanoparticles and Graphite. *Appl. Phys. Lett.* **2017**, *110*, No. 144101.
(41) Yang, C.; Gu, H.; Lin, W.; Yuen, M. M.; Wong, C. P.; Xiong, M.; Gao, B. Silver Nanowires: From Scalable Synthesis to Recyclable Foldable Electronics. *Adv. Mater.* **2011**, *23*, 3052−3056.

https://dx.doi.org/10.1021/acsami.1c01721
ACS Appl. Mater. Interfaces 2021, 13, 13724−13734